P. Brambilla, A. Guardone
Assessment of Dynamic Adaptive Grids in Volume-Of-Fluid Simulations of Oblique Drop Impacts onto Liquid Films
Journal of Computational and Applied Mathematics, Vol. 281, 2015, p. 277-283
doi:10.1016/j.cam.2014.12.030

Assessment of Dynamic Adaptive Grids in Volume-Of-Fluid Simulations of Oblique Drop Impacts onto Liquid Films

P. Brambilla, A. Guardone*

Department of Aerospace Science and Technology, Politecnico di Milano
via La Masa 34, 20156 Milano, Italy

Abstract

Grid spacing dependence in three-dimensional numerical simulations of non-normal drop impact onto thin liquid films is assessed for different impingement angles and grid refinement levels. To describe the liquid phase dynamics, the Navier-Stokes equations are coupled to a Volume-Of-Fluid (VOF) model. Numerical simulations are performed with a modified version software OpenFOAM over a structured grid of hexaedra. Grid adaptation is carried out using an edge subdivision technique which results in non-conformal meshes. Grid convergence is assessed by monitoring integral parameters describing the dynamics of the post-impact free-surface waves. Starting from an initial grid spacing between $D/8$ and $D/5$, with D drop diameter, a refinement level of three is found to be sufficient to describe the diverse flow feature and to identify the splashing regime.

Keywords: Drop impact, Two-phase flow, Dynamic adaptive grids, Volume-Of-Fluid, OpenFOAM

1. Introduction

The evaluation of the dynamics of a liquid drop impacting onto a liquid film of the same fluid is of paramount importance in both scientific and technical applications, including for example chemicals production, ink jet printing and fuel injection in combustion engines. Worthington was the first to investigate drop splashing into liquid film in 1908 [1]. More recently, from experimental results, Yarin and Weiss introduced a criterion to characterize normal drop impacts and an empirical relation describing the evolution of the radius of the crown in time [2]. Oblique drop impacts of interest here were investigated experimentally in [7, 8].

*Corresponding author
Email address: alberto.guardone@polimi.it (A. Guardone)

The numerical simulations of drop impact required the development of multi-phase solvers capable of capturing the drop-film interaction, the occurrence of secondary droplets and the formation of dry regions over the solid surface. Two-dimensional or axysimmetric numerical simulations of normal drop impact were performed in [3, 5]. Oblique drop impacts were simulated under the two-dimensional approximation in [6]. In 1999, Rieber and Frohn were the first to perform three-dimensional numerical computations of drop impacts whereby the drop trajectory is normal to the film surface [4]. In 2007, Nikolopoulos and collaborators simulated the same conditions studied by Rieber and Frohn using an adaptive grid technique [9]. Both References [4] and [9] used a Volume-Of-Fluid (VOF) technique to study normal drop impacts. Finally, in 2012, Brambilla and collaborators simulated for the first time oblique drop impacts onto liquid films in three spatial dimensions using dynamic adaptive grids [11].

The evaluation of the splashing dynamics in drop impact simulations calls for accurate spatial and temporal integration schemes as well as a very fine local spatial and temporal resolution to capture the liquid-gas interface. In particular, a fine grid spacing is mandatory if secondary droplet and corona breaking are to be correctly captured. In the present paper, the grid spacing requirements for normal and oblique drop impact simulations are assessed in connection to a novel dynamic adaptive grid VOF scheme implemented in the open-source CFD solver OpenFOAM (www.openfoam.org), see Ref. [11]. Grid convergence is monitored using the integral parameters describing the dynamics of the post-impact free-surface waves introduced in [11].

This paper is structured as follows. In section 2 the governing equations for the two-phase flow under scrutiny are introduced and the main feature of the OpenFOAM solver are briefly reported. In section 3, simulations results are discussed and a grid convergence study is presented. In section 4, final remarks and comments are given.

2. Governing Equations and Multi-phase solver

In the present work, the Volume-Of-Fluid (VOF) method of Hirt and Nichols [12]—a volume tracking method in which the interface is not described as a sharp discontinuity but instead is represented by an indicator function α, namely, the volume fraction of the dispersed phase—is used. As described in [13], in the OpenFOAM implementation the VOF scheme is rigorously derived from the so-called Euler-Euler approach, in which the Navier-Stokes equations are solved for two phases, which amounts to complement the single-phase model with an additional conservation law for the local concentration of the liquid phase. Therefore, the gas-liquid interface is an output of the solution procedure and its shape can be reconstructed a-posteriori by free-surface methodologies.

In each control volume, the volume fraction α varies in the interval $[0, 1]$,

where

$$\alpha = \begin{cases} 1 & \text{Liquid only} \\ 0 < \alpha < 1 & \text{Liquid-gas interface} \\ 0 & \text{Gas only} \end{cases} \tag{1}$$

The Navier-Stokes equations for incompressible flows of two immiscible fluids in the Euler–Euler formulation read

$$\begin{cases} \dfrac{\partial(\rho \boldsymbol{v})}{\partial t} + \nabla \cdot (\rho \boldsymbol{v} \otimes \boldsymbol{v}) = -\nabla p + \nabla \cdot \Sigma + \rho \boldsymbol{f} + \displaystyle\int_{S(t)} \sigma k' \boldsymbol{n'} \delta(x - x') dS \\ \dfrac{\partial \alpha}{\partial t} + \nabla \cdot (\alpha \boldsymbol{v}) = 0 \\ \nabla \cdot \boldsymbol{v} = 0 \end{cases} \tag{2}$$

where ρ is the density, $\boldsymbol{v}$ is the velocity vector, p is the pressure, $\boldsymbol{f}$ is the acceleration due to the volume forces, Σ is the stress tensor, σ is the surface tension coefficient, k is the surface curvature and $\boldsymbol{n}$ is the local normal. In incompressible flows of Newtonian fluids, $\Sigma = \mu[\nabla \otimes \boldsymbol{v} + (\nabla \otimes \boldsymbol{v})^{\mathrm{T}}]$, where μ is the kinematic viscosity. According to the VOF approximation considered here, the local values of ρ and μ in system (2) are computed as a linear combination of the liquid and gas values as

$$\rho = \alpha \rho_{\mathrm{L}} + (1 - \alpha)\rho_{\mathrm{G}} \qquad \text{and} \qquad \mu = \alpha \mu_{\mathrm{L}} + (1 - \alpha)\mu_{\mathrm{G}},$$

where the subscripts L and G indicate liquid and gas values, respectively. To model the effects of the surface tension (last term of the first equation of system (2)), the Continuum Surface Force (CSF) model of Brackbill et al. [14] is used.

System (2) governing the fluid motion is integrated using the solver *interDyMFoam* included in the OpenFOAM suit, which implements the VOF method. The solver allows to use a dynamic grid refinement technique through the *dynamicMesh* utility. The refinement technique is based on the Jasak's and Jasak and Gosman's h-refinement approaches [16, 17]. At each refinement step the edge of the cell is split into two in every direction, so that eight new cells are inserted in place of the initial cell. The cells marked for refinement are those containing the interface, that is with a value of α between 0 and 1. The *blockMesh* dictionary is used to generate the initial grid and the *setFields* dictionary sets non-uniform initial conditions such as for the phase fraction α in this case. The initial conditions are assigned on the unrefined grid. The modified procedure presented in [11] is used to refine the grid across the interface before the computation starts. In particular, the initial grid is refined using the initial solution until the maximum level of refinement is attained at the gas-liquid interface. Then, the initial condition is re-applied in the refined mesh and the computation starts.

The artificial compression term in the interFOAM solver is activated to reduce the thickness of the gas-fluid interface. A first order implicit backward Euler scheme is used to approximate the time derivative terms, a second order

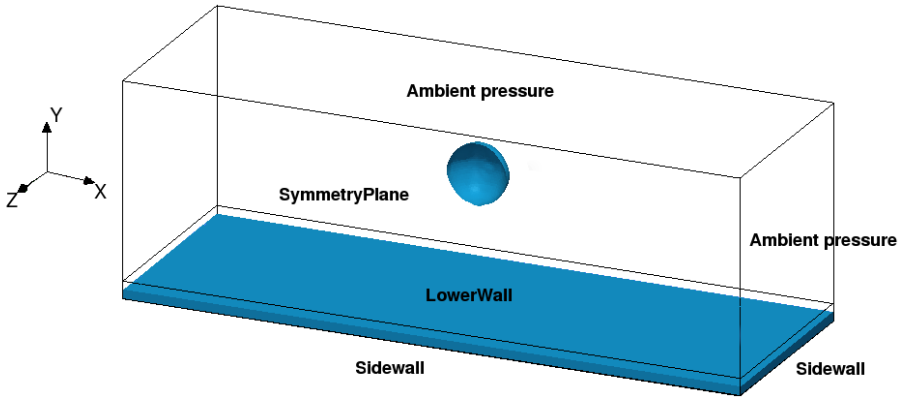

Figure 1: Computational domain with initial and boundary conditions. The distance between the drop center of gravity and the center of the film surface is $2.5D$ in all simulations.

Gaussian integration is performed to compute the spatial gradient, the Laplacian and the advection terms. A linear interpolation scheme is used during mesh adaptation. In all computations the Courant-Friederichs-Lewy number is equal to 0.3. Courant-Friederichs-Lewy number was kept ≤ 0.3, as suggested by OpenFOAM developers for 3D simulations, see [15].

3. Numerical simulations of oblique drop impacts

Numerical simulations of the oblique impact of a liquid drop onto a liquid film are presented in this section. The numerical simulations cover a range of impingement angles β from 10° to 90°. In all cases under scrutiny, the Weber number We is equal to 250, where

$$\mathrm{We} = \frac{\rho_\mathrm{d} D V_\mathrm{d}^2}{\sigma},$$

with ρ_d liquid density, D drop diameter, V_d drop velocity and σ surface tension. The Ohnesorge number Oh is equal to 0.0014 in all simulations, where

$$\mathrm{Oh} = \frac{\mu_\mathrm{d}}{\rho_\mathrm{d} \sigma D},$$

with μ_d dynamic viscosity of the liquid. The dimensionless film thickness H=h_0/D, where h_0 is the film thickness, is 0.116. The initial distance between the drop center of gravity and the center of the film surface is $2.5D$ in all simulations.

The symmetry with respect to the x-y plane, where the x-axis is parallel to the initial drop velocity and the y-axis is normal to the film surface, is enforced to reduce the size of the computational domain. The film liquid is constrained by three side walls and a lower wall located at $y = 0$, see Figure 1.

β [°]	L_x/D [-]	$\Delta h/D$ [%]
10	17.0	1.3281
20	16.0	1.2500
30	15.0	1.1719
40	14.4	1.1250
50	12.8	1.0000
60	11.2	0.8750
80	10.4	0.8125
90	9.6	0.7500

Table 1: Domain size along the x axis parallel to the initial drop velocity and maximum resolution $\Delta h/D$ achieved in each case, with Δh maximum linear dimension of the elements.

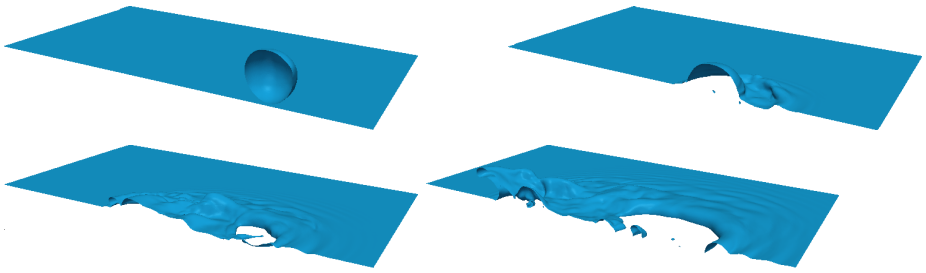

Figure 2: Computed gas-liquid interface for $\beta = 20°$ and We=250 at dimensionless time = -0.04; 1.46; 3.46; 5.96.

In all simulations, the domain extends to $3.58D$ in both y and z directions to reduce the influence of the walls. The x dimension L_x changes according to the impingement angle, since the spatial evolution of the impact in the longitudinal direction decreases with the increase of the impingement angle.

The initial grid is made of 46 080 elements ($80 \times 24 \times 24$). The initial resolution is $D/7$ in the y and z directions in all cases. In the x direction, the initial spacing is $D/5$ for $\beta \leq 30°$, $D/6$ for $30° < \beta \leq 50°$, $D/7$ for $50° < \beta \leq 60°$ and $D/8$ for $\beta > 80°$. The different initial resolutions of the considered grids are within one refinement level, namely, the ratio between the finest and coarser resolution is less than two in all cases.

To perform the grid refinement study, three different refinement levels equal to 2, 3 and 4 are considered. The maximum resolutions for each case are reported in Table 1. The dimensionless total time of the simulation $\tau = tV_\mathrm{d}/D$ is equal to 10 in all cases.

Figures from 2 to 5 show the computed gas-liquid interface for four different impingement angles with a refinement level of four. The reference dimensionless time τ_0 corresponds to the time at which the contact between the drop and the liquid film occurs. The impact dynamics differs significantly in the considered cases. At impingement angles less than about 40°, the formation of a ship prow-like structure is observed, as described by Okawa and collaborators in

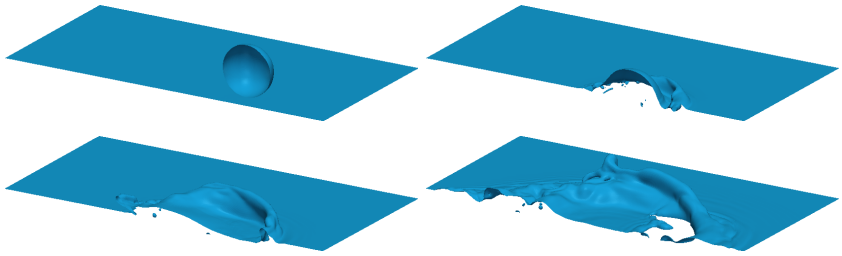

Figure 3: Computed gas-liquid interface for $\beta = 40°$ and We=250 at dimensionless time = -0.22; 0.78; 1.78; 3.78.

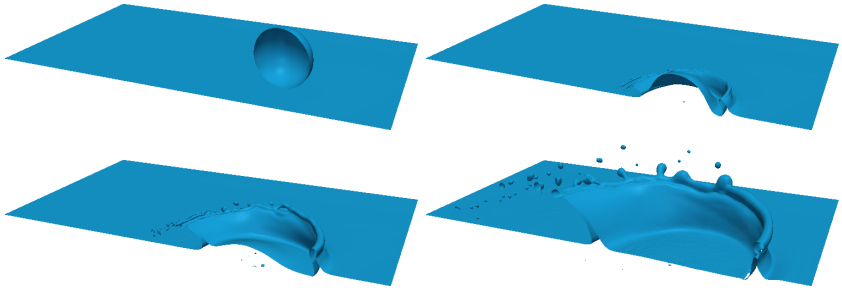

Figure 4: Computed gas-liquid interface for $\beta = 60°$ and We=250 at dimensionless time = -0.42; 0.58; 1.08; 2.58.

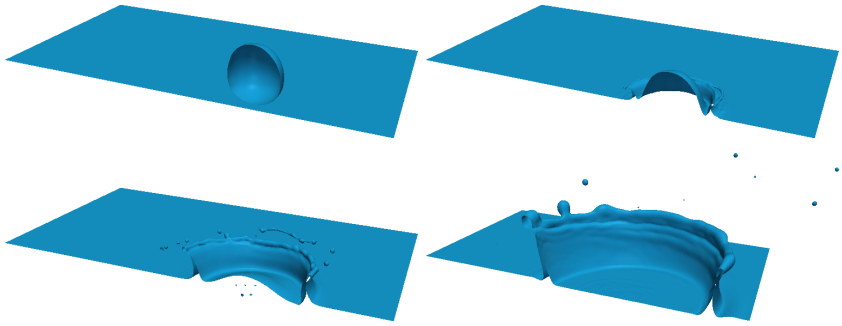

Figure 5: Computed gas-liquid interface for $\beta = 80°$ and We=250 at dimensionless time = 0.01; 1.01; 2.51; 4.01.

[10]. At impingement angles greater than 40°, the formation of a crown is observed after the impact. The crown has an asymmetric shape which tends to become symmetric as the impingement angle increases. At 90°, the corona shape is mostly axisymmetric around the center of impact, apart from interface instabilities and separating droplets.

Integral parameters were proposed in [11] to describe the evolution of the splashing front. These are the centres of gravity of the forward and backward portion of the corona, which are computed at each time step. The trajectories of the centres of gravity are reported in figure 6 for all considered impact angles and grid resolutions. The asymmetry of the crown can be appreciated in the case of angled impact; at $\beta = 90°$, see figure 6(h), the two curves overlap since the corona is symmetric. The backward portion of the front is more difficult to capture numerically because it involves a smaller fraction of the liquid and also because front instabilities occurs earlier with respect to the forward portion. Front instabilities, possibly resulting in front break-up and in the formation of secondary droplet, are responsible for the non linearity of the front trajectory observed in most conditions, see figure 6.

The trajectories of the centres of gravity of the forward and backward portions of the front are considered here to assess grid convergence in drop impact simulations. From figure 6, it is apparent that, for impingement angles lower than 40°, a refinement level of 2 delivers trajectories that are not in agreement with those obtained from refinement levels 3 and 4.

The trajectory of the forward portion of the front obtained from the grid with refinement level of 3 are almost coincident with that computed over the grid with refinement level 4, in particular within a distance of $1.5D$ from the center of impact, thus indicating that a good grid convergence is obtained already with a refinement level of 3, as far as this integral quantity is concerned. A different situation is observed instead for the backward portion of the front, where grid convergence is not observed even close to the impact point. However, for impact angles larger than 20 °, the considered grids agree in predicting the occurrence of a significant deviation from the initial straight trajectory at a distance between $0.5D$ and $1D$ from the center of impact, which is related to the front instability.

Table 2 reports a comparison of the computational time associated with the three resolutions under scrutiny. The indicated CPU time is made dimensionless by that required to complete the normal impact simulation with a refinement level of 2, which amounts to 7 722 s (2h 8m 42s) over 8 cores of a computer with two six-core Xeon 2.66 GHz CPU and 32 GB RAM. Note that the computations with a refinement level of 4 were carried out on 32 cores, thus computational times cannot be directly compared to a refinement level of 2 and 3, which were obtained with 8 cores. By increasing the refinement level from 2 to 3, the computational time is increased by a factor in between 14 and 20.

Table 3 reports the maximum number of cells resulting from the application of the adaptive procedure against that of a uniform grid with the same minimum grid spacing, for all considered impact angles and refinement levels. In all cases the use of adaptive grid techniques requires a number of elements that is lower by a factor of approximately 10, 20 and 30 for a refinement level of 2, 3 and 4,

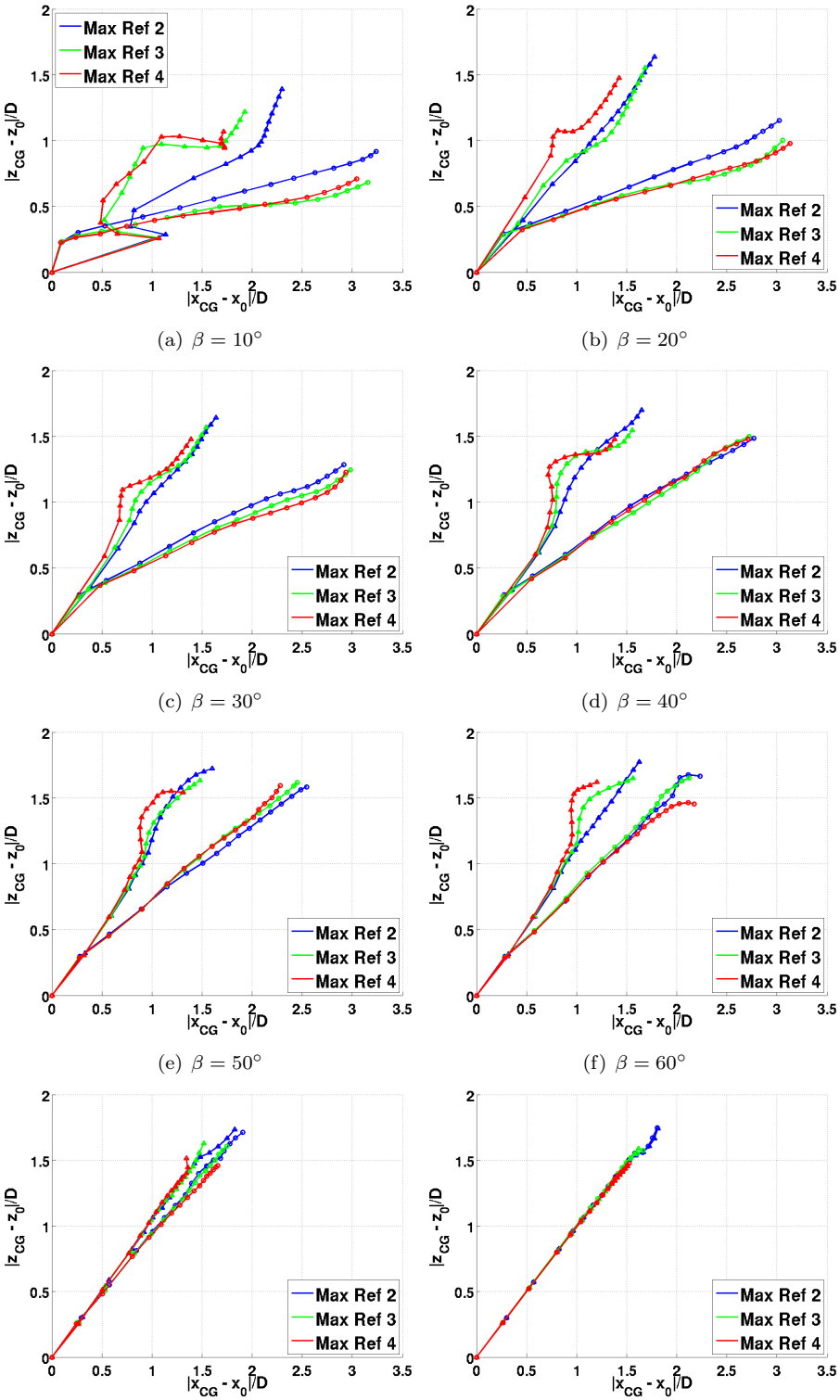

(a) $\beta = 10°$ (b) $\beta = 20°$

(c) $\beta = 30°$ (d) $\beta = 40°$

(e) $\beta = 50°$ (f) $\beta = 60°$

(g) $\beta = 80°$ (h) $\beta = 90°$

Figure 6: Trajectory of the centre of gravity: (◯) front and (△) back.

	CPU time [-]		
β [°]	Ref. 2 (8 Cores)	Ref. 3 (8 Cores)	Ref. 4 (32 Cores)
10	0.4	7.1	134.7
20	0.4	7.7	96.2
30	0.5	8.5	111.4
40	0.8	12.5	117.4
50	0.7	16.1	117.4
60	1.1	15.5	143.1
80	0.7	11.3	133.3
90	1.0	19.0	137.0

Table 2: CPU time requested to complete the numerical simulations at each impingement angle and refinement level. The CPU time is scaled with the value of 7722 s, which is the time required to complete the normal impact simulation with a refinement level of 2 over 8 cores of a computer with two six-core Xeon 2.66 GHz CPU and 32 GB RAM. Note that the computations with Ref. 4 (last column on the right hand side) were carried out on 32 cores, thus cannot be directly compared to Ref. 2 and Ref. 3 that were obtained with 8 cores.

	Grid elements (millions)					
	Ref. 2		Ref. 3		Ref. 4	
β [°]	Adapted	Uniform	Adapted	Uniform	Adapted	Uniform
10	0.26	2.98	1.19	23.81	5.76	188.01
20	0.26	2.95	1.18	23.59	5.74	188.74
30	0.27	2.90	1.23	23.78	6.35	188.01
40	0.28	2.92	1.24	23.36	6.26	188.98
50	0.31	2.95	1.35	23.59	6.62	188.74
60	0.34	2.99	1.51	23.53	7.02	188.27
80	0.35	2.97	1.51	23.77	7.09	188.63
90	0.36	2.92	1.53	23.71	7.09	188.27

Table 3: Number of computational cells at different angle of impact β. The maximum number of elements during the simulation is reported in the column Adapted; the column labeled Uniform reports the corresponding number of elements for an equivalent uniform grid with the same minimum spacing.

respectively, than that associated to a uniform grid with the same resolution.

4. Conclusions

A dynamic grid refinement method was applied to three-dimensional numerical simulations of oblique drop impact on a thin liquid layer. In particular, the computational grid was refined in the region containing the liquid-gas interface using an edge division approach, resulting in a non-conformal grid. Three different refinement level were considered, resulting from a maximum of 2, 3 and 4 edge divisions, respectively. A modified version of the solver *interDyMFoam* included in the OpenFOAM suit was used in all computations. The modified solver is capable of adapting the grid to the initial conditions to minimize the interpolation error.

Starting from an initial grid spacing between $D/8$ and $D/5$, with D drop diameter, a refinement level of three is found to be sufficient to describe the trajectory of the center of gravity of the forward and backward portion of the splashing front, in both the corona or drop spreading regimes. The dynamic mesh adaptation techniques allowed to significantly reduce the computational time with respect to fixed-grid computations, to the point of making it feasible to carry out the present parametric study on a relatively small computational cluster.

Future research activities will focus on the development of a reduced order model of oblique drop impact to be used in e.g. in-flight icing simulations over aircraft.

[1] A. M. Worthington, *A Study of splashes*, 129 pp. Longmans, Green, London (1908)

[2] A. L. Yarin and D. A. Weiss, *Impact of drops on solid surfaces: self-similar capillary waves and splashing as a new type of kinematic discontinuity*, J. Fluid Mech., 283, 141-173 (1995)

[3] D. A. Weiss and A. L. Yarin, *Single drop impact onto liquid films: neck distortion, jetting, tiny bubble entrainment and crown formation*, J. of Fluid. Mechanics, 385, 229-254 (1999)

[4] M. Rieber and A. Frohn, *A numerical study on the mechanism of splashing*, Int. J. of Heat and Fluid Flow, 20, 455-461 (1999)

[5] C. Josserand and S. Zaleski, *Droplet splashing on a thin liquid film*, Physics of Fluids, 15(6), 1650-1657 (2003)

[6] R. Purvis and F. T. Smith, *Large droplet impact on water layers*, AIAA Paper, 2004-414 (2004)

[7] D. W. Hammond et al., *Analysis and experimental aspects of the impact of supercooled water droplets into thin water films*, AIAA Paper, 2005-0077 (2005)

[8] M. Quero et al., *Analysis of super-cooled water droplet impact on a thin water layer and ice growth*, AIAA Paper, 2006-466 (2006)

[9] N. Nikolopoulos et al., *Three-dimensional numerical investigation of a droplet impinging normally onto a wall film*, J. of Computational Physics, 225, 322-341 (2007)

[10] T. Okawa et al., *Effect of the impingement angle on the outcome of single water drop impact onto a plane water surface*, Exp Fluids, 44, 331-339 (2008)

[11] P. Brambilla et al., *Automatic tracking of corona propagation in three-dimensional simulations of non-normal drop impact on a liquid film*, Computing, 95:5, 415-424 (2013)

[12] C. W. Hirt and B. D. Nichols, *Volume of fluid (VOF) method for the dynamics of free boundaries*, J. of Computational Physics, 39, 201-225 (1981)

[13] S. S. Deshpande et al. , *Computational and experimental characterization of a liquid jet plunging into a quiescent pool at shallow inclination*, International Journal of Heat and Fluid Flow, 34, 1-14 (2012)

[14] J. U. Brackbill et al., *A continuum method for modelling surface tension*, J. of Computational Physics, 100, 335-354 (1992)

[15] H. Jasak et al., *Volume of fluid methods for immiscible-fluid and free-surface flows*, Chemical Engineering Journal, 141, 204-221(2008)

[16] H. Jasak, *Error analysis and estimation for the finite volume method with applications to fluid flows*, PhD. Thesis, Imperial College, University of London, 1996.

[17] H. Jasak and A. D. Gosman, *Automatic resolution control for the finite-volume method, part 2: adaptive mesh refinement and coarsening*, *Numerical Heat Transfer, part B, 38(3):257-271*, 2000.